Received 14 December 2020; accepted 29 December 2020. Date of publication 6 January 2021; date of current version 22 January 2021.

Digital Object Identifier 10.1109/OJCOMS.2020.3048954

Performance Analysis of Indoor Communication System Using Off-the-Shelf LEDs With Human Blockages

ANAND SINGH [1] (Graduate Student Member, IEEE), GOURAB GHATAK [1] (Member, IEEE), ANAND SRIVASTAVA[1], VIVEK ASHOK BOHARA [1] (Senior Member, IEEE), AND ANAND KUMAR JAGADEESAN[2]

[1]Department of Electronics and Communication Engineering, Indraprastha Institute of Information Technology Delhi, New Delhi 110020, India

[2]Cognizant, Chennai 600096, India

CORRESPONDING AUTHOR: A. K. JAGADEESAN (e-mail: anandsi@iiitd.ac.in)

ABSTRACT This article uses a stochastic geometry model-based approach to analyze the downlink performance of an indoor visible light communication (VLC) system with human blockages. The system performance is analyzed for a regular placement of light emitting diodes (LEDs) in a rectangular configuration. The proposed analysis is divided into two parts. In the first part, it is assumed that human blockages are static. The closed-form expression of the signal-to-noise ratio (SNR) at the receiver with static human blockages is derived. Further, the analysis is extended for the case where blockage mobility has also been considered. We compare the system performance in terms of received SNR for 4 and 8 LED configurations under predefined total power constraint. It is observed that at a lower density of human blockages in the room, the 4-LED configuration outperforms the 8-LED configuration. However, at a higher density of human blockages in the room, the 8-LED configuration outperforms the 4-LED configuration for the same total power constraint. Hence the proposed analysis will be useful for designing a VLC based indoor communication system wherein the system designer can switch between these two configurations depending on the number of blockages.

INDEX TERMS Visible light communication (VLC), human blockage, matern hardcore point process (MHCP), random waypoint model (RWP).

I. INTRODUCTION

THE SHORTAGE of spectrum in the conventional ultra-high frequency (UHF) bands coupled with increasing wireless data traffic has led the researchers to consider employing visible light communication (VLC) as one of the candidate technologies to facilitate high throughput communication in the next-generation wireless cellular standards. In this regard, integration of 5G New Radio with a VLC system to support the cellular downlink architecture has been proposed in the literature [1], [2]. Further, to cater to these high throughput application scenarios, both back-haul and wireless front-ends need to be improved [3]. Recent studies have shown that the demand is much more severe in indoor communication, where the maximum data usage occurs [4]. Hence, VLC is an optical wireless communication technology that can be used to fulfill the high capacity demand in indoor scenarios. In a VLC system, a light-emitting diode (LED) is used as a transmitter, while a photo-detector (PD) is used as a receiver. The system operates on an intensity modulation/direct detection (IM/DD) scheme in which the intensity of LED is modulated to carry the information, and the optical signal is detected directly by a photodiode. License-free deployment and nearly universal LED availability make it an attractive and inexpensive choice for the service providers [5].

LEDs have a modulation bandwidth of up to 20 MHz, which can support very high data rates. Moreover, it has been shown that one can achieve higher capacity and more

secure communication using VLC [1], [6]–[8]. It allows significant power savings as the visible light sources can serve the dual role of communications and illumination. However, despite its numerous advantages, it has few drawbacks, such as it suffers from high interference from other light sources and is prone to significant losses due to blockage [9]. Therefore, it is essential to include the impact of users' locations and modeling of the human blockages in the performance analysis of a VLC system.

The received optical power in the indoor VLC system depends on the distance between the transmitting LEDs and the desired user inside the room. In a multi-user scenario, the other users inside the room act as blockages for the desired user. These blockages result in a sudden fall in the received optical power as it can block both the line-of-sight (LoS) and the non-line-of-sight (NLoS) signal from the LED to the desired user. The amount of power reduction will depend on the height and width of the blockage. In order to analyze the impact of static and dynamic human blockages in indoor VLC systems performance, we have employed stochastic geometry-based probabilistic models to characterize the human blockages. The first model uses the Matern hardcore point process (MHCP) to realize the static blockages. In MHCP, two or more blockages are separated by an absolute minimum distance to avoid overlapping them. Further, to include the effect of dynamic human blockages moving with a uniform velocity inside the room, the random waypoint (RWP) model is utilized. In this letter, the received optical power with respect to blockage density across the room is analyzed for 4, and 8 LED rectangular configurations. Additionally, this letter analytically determines the signal-to-noise ratio (SNR) at the receiver for MHCP configuration using stochastic geometry for human blockages' varying intensity.

A. RELATED WORK

Stochastic geometry has emerged as a tractable approach to analyze wireless systems, and it has been recently applied to analyze VLC networks. In [10], the authors have characterized the data rate and coverage of different radio frequency (RF) and VLC systems under different configurations using stochastic geometry. A novel cooperative transmission and reception scheme in VLC is proposed and evaluated in [11], where neighboring attocells smartly cooperate to decrease the probability of blockage in the LoS link. The scheme proposed in [11] provides improvements and reliability in large indoor scenarios, such as corridors, laboratories, shops, and conference rooms, where the coverage needs to be obtained by using different access points when VLC is used. However, [11] does not consider the effect of blockages inside the room in their analysis. In order to overcome the conventional positioning problems, as well as to improve the positioning accuracy and to expand the service area, a new hybrid positioning methodology is proposed in [12]. Two design techniques for an environment-friendly positioning system are proposed and developed. These methods use a hybrid VLC scheme with an extremely low reception error and a Zigbee mesh wireless network. However, in [12], the authors only considered the LoS link in the absence of human blockage while calculating the received signal power in the system. In [13], a novel and tractable model for characterizing the probability of human-body blockage is proposed. Specifically, they model the humans as cylindrical objects with arbitrarily distributed heights and radius, whereas the center of the cylinder follows a Poisson Point Process (PPP) in two dimensions (2-D). A novel access point (AP) placement method that considers a stationary distribution of the users has been proposed in [14]. This distribution is the result of the mobility pattern of the users in an indoor environment. The proposed method is independent of the resource allocation algorithm and eliminates the need for exhaustive simulations to find the optimal location for VLC APs. In an indoor environment, depending on their mobility pattern, the users may be reluctant to stay close to the walls, and the distribution of the users is generally not uniform. For example, users' stationary distribution is well approximated by an elliptic paraboloid function if the users obey the random waypoint mobility model [15]. Dastgheib *et al.* have introduced the problem of mobility-aware optimization of resources in VLC networks using the T-step look-ahead policy and employing the notion of handover efficiency in [16]. It is shown that the handover efficiency can be correlated with future actions based on users' mobility. In [17], the authors investigated the deployment of light sources and proposed an optimization framework for power allocation to evaluate the bit-error-rate (BER) and the required transmitted signal power under illumination constraints in the presence of blockages. The system performance is further optimized under lighting constraints, especially when a blockage impairs the LoS link. A low complexity optimization problem is formulated wherein a simplified power allocation is derived.

Further, to track the behavior of the mobile users, it is essential to use a mobility model such as random walk [18], Markovian models [19], Levy walk [20], and models based on product-form queuing networks [21], [22]. Amongst different models, the RWP is widely used, and hence is thoroughly studied [15]. In RWP model, each user moves at a uniform velocity. Further, it selects another destination randomly according to a uniform distribution and moves toward that point with another velocity along a straight line [23]. As the users continue to move, the distribution of users' position approaches a stationary distribution [15]. For the dynamic users inside the room, the fact is that most of the users will prefer to stay at the center of the room rather than near the edge of the room or close to walls. The RWP model results in a distribution concentrating more probability mass near the center of the coverage area. Therefore, most of the optical power in VLC is concentrated near the placement of LED, and it is more reasonable to employ the RWP mobility model rather than uniform spatial distribution. Further, for an efficient VLC system, it is essential

to analyze its performance with user movements. It will be interesting to observe the indoor VLC system behavior with blockages, including NLoS links, which have not been explored previously in the literature.

B. CONTRIBUTIONS AND OUTLINE

Earlier works on indoor VLC systems have not considered humans' impact as a blockage. Further, the existing work ignores the effect of static and dynamic human blockages inside the room. The indoor VLC system with human blockages, including NLoS links, has not been explored previously in the literature. The above study will also not provide any method to characterize the static and dynamic blockages inside the room. Our study tries to address all the above-mentioned research gaps in this letter.

In the proposed work, we analyze an indoor VLC system in the presence of static and dynamic human blockages. The performance is demonstrated for fixed placement of LEDs in a rectangular configuration with 4 LEDs and 8 LEDs arrangement. For the realization of static and dynamic human blockages, we have used the Matern hardcore point process (MHCP) and random waypoint model (RWP), respectively. In MHCP, two or more points are separated by an absolute minimum distance to avoid overlapping between them. This also reflects a practical scenario for static human blockages wherein two or more blockages does not overlap. While the density of human blockages are independent of the room size, it may be noted that the number of blockages are directly proportional to the area of the room. The employed MHCP model has also been conventionally used to plan the deployment and modeling of blockages and interference calculation in wireless and VLC networks [24]. Similarly, the RWP mobility model is a simple stochastic model that describes a human blockage's movement behavior in a given room [25].

The main contributions of the work are summarized as follows:

- We adopt a stochastic-geometry based approach to study the performance of an indoor VLC system in the presence of human blockages. In particular, we consider two models of blockages: static and mobile and characterize the impact of the density of the blockages on the received signal strength of a receiver uniformly placed inside the room. Contrary to the existing studies on indoor VLC systems, which typically ignore the impact of human blockages, our investigation reveals that the blockages considerably impact the propagation environment and significantly alters the system design insights.
- Then, we extend our study to the MHCP with different radii to emulate different sizes of the blockages. Further, to include blockages' movement, the RWP model with uniform velocity has been considered. The RWP model gives more practical realizations of blockages inside the room.
- Furthermore, we investigate the effect of the number of LEDs on the system performance by considering two LED configurations, consisting of 4 and 8 LEDs. Interestingly, our study shows that for lower blockage densities, the 4 LED configuration results in a higher received power, whereas for higher blockage densities, the operator should switch to a 8 LED configuration to maintain the desired receiver QoS.

The proposed performance analysis of the VLC system in the presence of static and dynamic blockage can be used in a practical environment like offices, factories, and malls with stationary blockage (like furniture or a human with no mobility) and dynamic blockages (moving with uniform velocity). One can adopt the 4 or 8 LED configuration depending on the desired QoS, such as minimum BER, outage, or maximizing data rate.

The rest of this article is organized as follows. In Section II the system model is described which includes VLC channel model and spatial model of human blockages. The analytical framework for blockage realization using MHCP is derived in Section III. Section IV gives a characterization of human blockages using the RWP model. The analytical expression of SNR at the receiver with human blockages is derived in Section V. The analytical and simulation results have been discussed in Section VI. Finally, Section VII concludes this article.

Notations: The vector and the matrix are denoted as boldface as $\mathbf{x}$ and $\mathbf{X}$, respectively. $\mathbf{x}^T$ and $\mathbf{X}^T$ denote the transpose of vector $\mathbf{x}$ and matrix $\mathbf{X}$. The vectorization of matrix $\mathbf{X}$ is denoted as $\mathbf{X}(:)$. The element corresponding to i^{th} row and j^{th} column of a matrix $\mathbf{X}$ is represented as X_{ij}. The cumulative distribution function (CDF) of the random variable is denoted as F. The retaining and blockage probabilities are represented as P_{retain} and P_B, respectively. The expectation of the random variable is denoted as E. The set of positive real numbers is denoted by $\mathbb{R}^+$ and $\mathbb{R}^2$ denotes the two-dimensional space. Φ denotes the set of points in the Poisson point process (PPP). The intensity of the point process is defined by λ.

II. SYSTEM MODEL

As mentioned before, we consider two scenarios of 4 and 8 LEDs in the rectangular configuration in a 5 m $\times$ 5 m $\times$ 3 m room. The receiver plane is assumed to be 0.85 m above the floor. Both LoS and NLoS paths are considered. The receiver plane is divided into a 25 $\times$ 25 grids to cover the whole room for analysis. We have used the Matern type-II process and RWP model to distribute the location of the static and dynamic blockages in a plane with an intensity of λ_B respectively. The blockages are assumed to be cylindrical with radius r and the height h_B, as shown in Fig. 1(a). For the proposed system model, two types of blockages of having radius r_1 and r_2 have been considered, which are equivalent to varying sizes of humans. We have assumed OOK modulation in the VLC link for deriving the BER

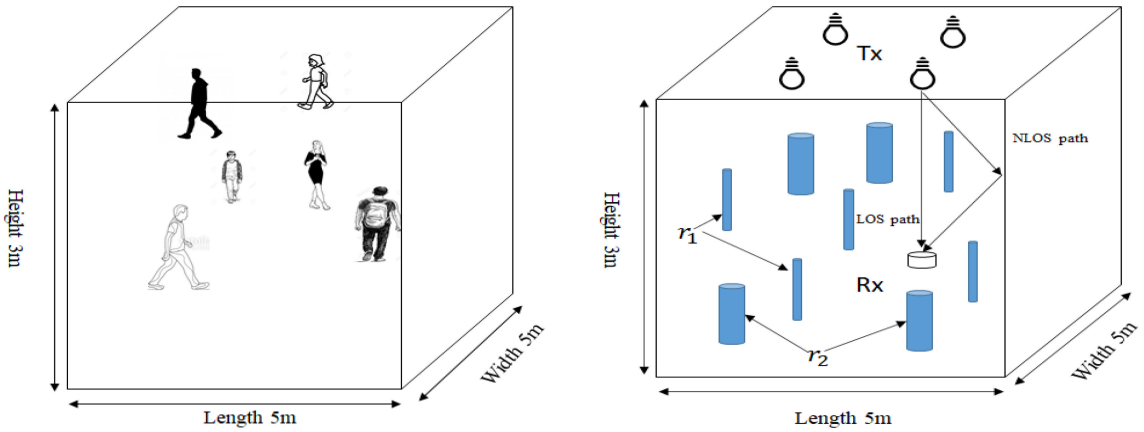

(a) Human blockage inside the room.

(b) Human blockages modeled as a cylinder.

FIGURE 1. System Model.

expression as this is one of the standards modulation scheme defined in the VLC standard (IEEE 802.15.7) [26].

In the following subsections, we discuss in detail the VLC channel and the spatial model of human blockages.

A. VLC CHANNEL MODEL

Lambert radiator is a typical radiation model that can model the LED light source in VLC [27]. Radiation patterns of few commercially available LEDs are assumed to be Lambertian. It has also been pointed out in [28], that the Lambertian model can accurately reproduce the LoS and NLoS luminous intensity pattern of the phosphor-coated multi-chip LEDs, the batwing LEDs, or the side-emitting LEDs. The frequency response of such a channel is given as [29]:

$$H(f) = H(0)\exp(-j2\pi f \Delta\tau_{LOS}) + H_{DIFF}\frac{\exp(-j2\pi f \Delta\tau_{DIFF})}{1+j\left(\frac{f}{f_0}\right)}, \quad (1)$$

where $\Delta\tau_{LOS}$ and $\Delta\tau_{DIFF}$ are the time delays of the transmitted signal taking the LoS and the NLoS path, respectively and f_0 denotes the cut-off frequency of scattering channel. $H(0)$ is the channel gain of LoS component, which is given as:

$$H(0) = \begin{cases} \frac{(m+1)A}{2\pi D_d^2}\cos^m(\phi)T_s(\psi)g(\psi)\cos(\psi) \\ 0 \le \psi \le \psi_c \end{cases}, \quad (2)$$

where m represents Lambertian order defined as:

$$m = \frac{-ln(2)}{ln\left(cos\left(\phi_{\frac{1}{2}}\right)\right)}. \quad (3)$$

In (2), A is the physical area of the PD, D_d is the distance between the VLC transmitter and the receiver, ψ is the angle of incidence, ϕ is the angle of irradiance, ψ_c is the receiver FOV, $T_s(\psi)$ is the gain of the optical filter, and $g(\psi)$ is the gain of the optical concentrator given as:

$$g(\psi) = \begin{cases} \frac{n^2}{\sin^2(\psi_c)}, & 0 \le \psi \le \psi_c, \end{cases} \quad (4)$$

where n is the refractive index of optical concentrator and $\phi_{\frac{1}{2}}$ is LED half beam angle. The diffuse channel gain H_{DIFF} due to NLoS path is given as:

$$H_{DIFF} = \frac{A_R}{A_{room}}\frac{\rho}{1-\bar{\rho}}, \quad (5)$$

where,

$$\bar{\rho} = \frac{1}{A_{room}}\sum_i A_i\rho_i, \quad (6)$$

$\bar{\rho}$ represents an average reflectance, ρ refers to instantaneous reflection, A_R is the area of reflection point on the wall from where the NLoS rays are reflected inside the room, A_i is the area of i_{th} grid on the wall and A_{room} is the total area of the room.

For a given transmission power (P_T), the total received power using multiple LEDs including diffused path through the walls can be obtained as:

$$P_r = \sum_{i=1}^{N}\left[P_T H(0) + \int_{walls} P_T H_{DIFF}\right]. \quad (7)$$

where N is the total number of transmitting LEDs, and the total power is obtained by ingratiating both LoS the NLoS link across the room.

B. SPATIAL MODEL

Consider the scenario illustrated in Fig. 2, where a transmitter (Tx) is located at a certain height h_T above the ground, and a receiver (Rx) is located at a height h_R. The potential human blockages are distributed over the receiver plane. As stated before, we model the blockages as cylinders [30] with a certain height, h_B, and the base diameter of D. The

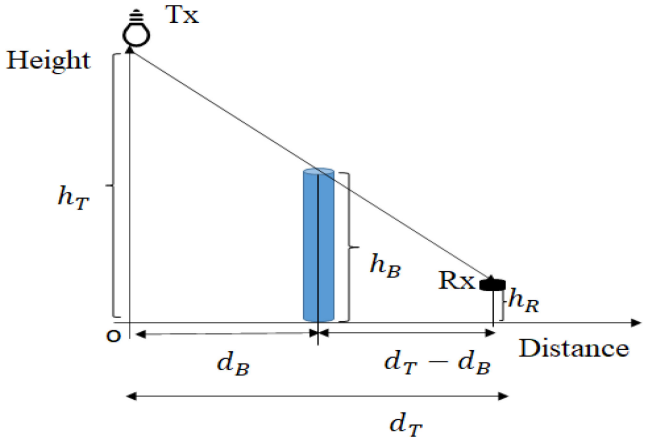

FIGURE 2. Schematic for calculation of shadow length due to blockage.

locations of the human blockages present inside the room are distributed as per the mobility aspects of humans.

As illustrated in Fig. 2, a human body of height h_B is present between the LED and the receiver, which results in a communication link blockage. The distance of the human blockage and the intended user from LED is denoted by d_B and d_T, respectively. Using simple geometry, (Fig. 2) the length of shadow due to blockage form LED $d_T - d_B$ can be calculated as:

$$d_T - d_B = \frac{h_B}{h_T} d_T. \tag{8}$$

The region in shadow due to blockage will be a rectangle whose area can be calculated using (8), with a length equal to $d_T - d_B$, and width similar to the blockage diameter D.

III. CHARACTERIZATION OF STATIC HUMAN BLOCKAGES USING MHCP

This section discusses the realization of the locations of the stationary human blockages inside the room using MHCP. The effect of homogeneous and heterogeneous blockages is analyzed. In MHCP, two or more points are forbidden to be closer than a certain minimum distance. The MHCP is also used to plan the deployment of base stations in cellular networks and modeling of blockages and interference calculation in wireless networks [24]. One way to achieve such a minimum distance between points is to start with a parent point process with no such restriction and then remove points that violate the above condition. We start with a target number of blockages (N_B) to be considered for the downlink analysis. To model the location of the blockages, we assume a modified version of the type-II MHCP process, wherein, the points are a result of random thinning of a parent PPP Φ_P with intensity λ_P. In particular, for each realization of Φ_P, we assign a random mark [0, 1] to each $\mathbf{x_i} \in \Phi_P$. Then, $\mathbf{x_i}$ is deleted if there exists an $\mathbf{x_j}$, $j \neq i$, such that the mark assigned to $\mathbf{x_j}$ is lower than the mark assigned to $\mathbf{x_i}$. Let the resulting MHCP so created be denoted by Φ_B with intensity λ_B. Finally, we check the condition $N_B = \Phi_B(A)$, and perform the downlink analysis of the network for only such realizations in which $N_B = \Phi_B(A)$ holds. we have used above describe MHCP to characterize the locations of stationary homogeneous (same radii r_1 or r_2) and heterogeneous (different radii r_1 and r_2) blockages, where $r_1 < r_2$.

A. INTENSITY OF HOMOGENEOUS BLOCKAGES USING MHCP

In this subsection, we have characterized the homogeneous blockage process having radius r_B using MHCP. First, a parent Poisson point process is generated to realize the locations of human blockages in a 2-D plane. A random point or mark is associated with each human blockage, and a point of the parent Poisson process is deleted if there is another mark within the hardcore distance of δ. The intensity of the resulting process is [24]:

$$\lambda_{B1} = \frac{1 - \exp(\lambda_p \pi \delta^2)}{\pi \delta^2}. \tag{9}$$

where λ_p is the intensity of the parent point process. As shown in Fig. 2, the link between two nodes located at a distance d_B from each other is blocked if a element of point process falls in the shadow region of the blockage. The probability that the center of at least one blocking object falls in the shaded the area can be calculated using the void probability [31]:

$$P_B(d) = 1 - \exp\left(-2\lambda_{B1} d_B r_B^2\right). \tag{10}$$

where λ_{B_1} is the blockage intensity having same radius and r_B is the blockage radius which can be either r_1 or r_2.

B. INTENSITY CALCULATION OF HETEROGENEOUS BLOCKAGES USING MHCP

This subsection has characterized the heterogeneous blockage process with radius r_1 and r_2 using MHCP. The blockages inside the room have been modelled in two steps. In the first step, the points with fixed radius r_1 and r_2 are generated and the respective weights are assigned as $W_1(r_1)$ and $W_1(r_1)$. This marked Poisson process we denoted by Φ, and a point of the marked process in $\mathbb{R}^2$ is denoted by $[x; r]$.

In the second step, we thin the marked point process by letting all pairs of points whose associated cylinders intersect compete. A point is kept if it has a higher weight in all pairwise comparisons. Given a pair of blockages points $[x_1; r_1]$, $[x_2; r_2] \in \Phi$, we give points independent weights, $W_1(r_1)$ and $W_2(r_2)$ respectively, which will depend on the radius, therefore, for the proposed model ($r_1 < r_2$), W_1 will be less than W_2. If their associated cylinder intersects, the point with the lower weight is removed, and the point with the higher weight will be retained.

Hence, the retaining probability of a typical point with radius r and weight W after thinning is [32]:

$$P_{retain}(r) = \mathrm{E}\left[\exp\left\{-\lambda_P \pi r^2 \int_0^\infty \{P(W_1(r) \leq W_2(y)\} \times (r+y)^2 F_{pr}(dy)\right\}\right], \tag{11}$$

where $W_1(r)$ and $W_2(y)$ are independent weights and F_{pr} is the distribution of radius before thinning. A point and its associated d-dimensional cylinder are kept if and only if the sphere meets no larger or equal sized sphere of the marked point process. Further, $E[P(W_1(r) \leq W_2(y))] = 1 \quad (r \leq y)$, then the retaining probability can be further written as:

$$P_{retain}(r) = \exp\left(-\lambda_P \pi r^2 \int_r^{\infty} (r+y)^2 F_{pr}(dy)\right). \quad (12)$$

We now consider a heterogeneous model of cylinders (blockages) with two different radius r_1 and r_2. Let P_1 and P_2 denote the probability of blockage with radius r_1 and r_2, respectively. The probability after thinning $P_{thin}(r_1)$ for the case $r_2 = 2r_1$, using [32, Th. 3.2 and Corollary 2.2] in (12). The retaining probability of blockage radius r_1 can be expressed as:

$$P_{retain}(r_1) = \frac{P_2(9P_1 + 16P_2)}{P_1(4P_1 + 9P_2)^{-1} + P_2(9P_1 + 16P_2)^{-1}}, \quad (13)$$

Similarly, the retaining probability of blockage radius r_2 can be expressed as:

$$P_{retain}(r_2) = \frac{P_1(4P_1 + 9P_2)}{P_1(4P_1 + 9P_2)^{-1} + P_2(9P_1 + 16P_2)^{-1}}. \quad (14)$$

The intensity of thinned point process with retaining probability $P_{retain}(r)$ is given by [32]:

$$\lambda_{th} = \lambda_P P_{retain}(r). \quad (15)$$

Using (13), (14) and (15), the equivalent blockage density $\lambda_{B2}(r)$ for heterogeneous blockage process are generated which are given as:

$$\lambda_{B2}(r_1) = \lambda_P \frac{P_2(9P_1 + 16P_2)}{P_1(4P_1 + 9P_2)^{-1} + P_2(9P_1 + 16P_2)^{-1}}, \quad (16)$$

$$\lambda_{B2}(r_2) = \lambda_P \frac{P_1(4P_1 + 9P_2)}{P_1(4P_1 + 9P_2)^{-1} + P_2(9P_1 + 16P_2)^{-1}}. \quad (17)$$

IV. CHARACTERIZATION OF DYNAMIC BLOCKAGES USING RWP

In this section, the dynamic effect of human blockages moving within the room with the uniform velocity has been analyzed. The RWP mobility model is a simple and straightforward stochastic model that describes a human blockage's movement behavior in given room size. In this model, a blockage randomly chooses a destination point ('waypoint') in the room and moves with uniform velocity on a straight line to the next destination point. After waiting for a specific pause time, it chooses a new destination and moves with uniform velocity to the destination, and so on. As discussed earlier, in a VLC system, the achievable user's data rate is related to the user-AP distance; therefore, including the spatial user distribution becomes essential.

Furthermore, note that human blockages are not necessarily distributed uniformly in typical indoor environments across the network area. On the contrary, their location distribution is characterized by a higher probability of being located near the center of the room than near the walls. Incidentally, the stationary distribution of the RWP model captures such a spatial configuration. For example, as discussed in [15], users' stationary distribution without pause-time in an RWP model can be approximated by an elliptic-paraboloid function.

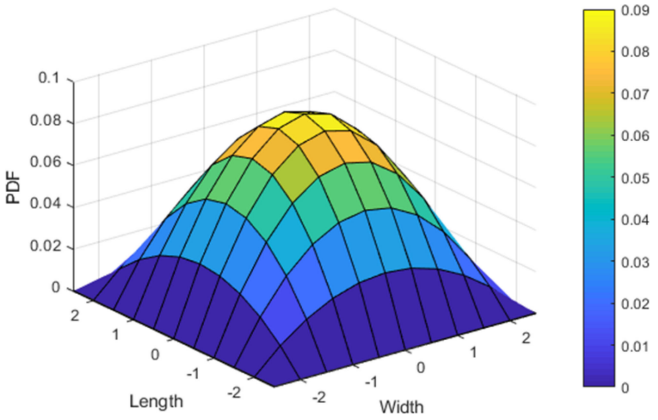

FIGURE 3. Stationary RWP model location PDF.

In the analysis, RWP model is considered in a rectangular area of size $R = a \times a$, a point (waypoint) S_1 is selected randomly in R. A pause time at point S_1 is chosen randomly in an interval $[t_{min}, t_{max}]$, upon the termination of pause time, a new waypoint S_2 is chosen uniformly at random in R, and the node starts moving from S_1 to S_2 along a straight line trajectory with velocity chosen uniformly at random in an interval $[v_{min}, v_{max}]$. The pause and movement process is repeated as above when the node arrives at the destination. For the sake of simplicity and without loss of generality, we have used the RWP model without any pause time. As the users continue to move, the distribution of the position of users approaches a stationary distribution. In particular, for a square area of size, $a \times a$, the stationary distribution of the user locations is:

$$f_X(\mathbf{x}) = f_{XY}(x, y) = \frac{36}{a^6}\left(x^2 - \frac{a^2}{4}\right)\left(y^2 - \frac{a^2}{4}\right), \quad (18)$$

where $\frac{-a}{2} \leq x \leq \frac{a}{2}$, $\frac{-a}{2} \leq y \leq \frac{a}{2}$ shows the coordinate of each node in the square area and $\mathbf{x} = [x \quad y]$ is the position vector. This stationary distribution is also represented in Fig. 3, which confirms the concentration of the users near the center of the room.

V. SNR MODEL

In this section, the received SNR is calculated for the stationary blockage process using MHCP. It is assumed that when the PD is in blockage, it receives no signal. The optical signal transmitted by the i_{th} LED is given by:

$$s_i(t) = P_{t_i}[1 + M_I x_i(t)], \quad (19)$$

where P_{t_i} is the transmit power at the i_{th} LED, x_i is the corresponding modulating OOK signal and M_I is the modulating index [33]. Here, the first term (P_{t_i}) in (19) takes

care of illumination while the second term ($P_{t_i} M_I x_i$) is for communication. After photo-detection, assuming that the DC component of the detected electrical signal is filtered out at the receiver, the received signal at photo-detector j is given by

$$y_j = \mathcal{R} P_{r_j} + n_j, \tag{20}$$

where $\mathcal{R}$ is photodiode responsitivity, n_j is additive white Gaussian noise (AWGN) with $n_j = \mathcal{N}(0, \sigma_j^2)$ and P_{r_j} is expressed as:

$$P_{r_j} = \sum_{i=1}^{N} H_{ij} P_{t_i} M_I x_i, \tag{21}$$

where N is the number of LEDs and H_{ij} is the VLC channel coefficient between i_{th} LED and j_{th} PD, using (2) H_{ij} and can be expressed as [5]:

$$H_{ij} = \frac{(m+1)\cos^m(\phi) A \cos(\theta)}{2\pi d_{ij}^2}. \tag{22}$$

where d_{ij} is the distance between the i_{th} LED and the j_{th} PD. If there is human blockage between the LED and the PD at distance d with probability $P_B(d)$ between transmitting LED and the PD the VLC channel gain with blockage can be expressed as:

$$\begin{aligned} H_{ij}^B &= H_{ij}[(1 - P_B(d))] \\ &= \frac{M\left[\exp\left(-2\lambda_B d_{ij} r_B^2\right)\right]}{2\pi d_{ij}^2}, \end{aligned} \tag{23}$$

where $M = (m+1)\cos^m(\phi) A \cos(\theta)$. The noise variance σ_j^2 at j_{th} PD is the total noise comprising of shot noise (σ_{shot}^2) and thermal noise ($\sigma_{\text{thermal}}^2$) which can be expressed as [34]:

$$\sigma_j^2 = \sigma_{\text{shot}}^2 + \sigma_{\text{thermal}}^2, \tag{24}$$

where

$$\sigma_{\text{shot}}^2 = 2e\mathcal{R} P_{\text{r}_\text{j}} B_s + 2e I_{\text{bg}} I_2 B_{\text{s}}, \tag{25}$$

and

$$\sigma_{\text{thermal}}^2 = \frac{8\pi k T_{\text{k}}}{G} \eta A_{\text{r}} I_2 B_s^2 + \frac{16\pi^2 k T_{\text{k}} \Gamma}{g_{\text{m}}} \eta^2 A_{\text{r}}^2 I_3 B_s^3 \ . \tag{26}$$

where e is the electron charge, P_{r_j} is the received optical power at j_{th} PD, B_{s} is the system bandwidth, I_{bg} is the received background noise current, k is Boltzmann's constant, T_{k} is the absolute temperature, G is the open loop voltage gain, η is the fixed capacitance of PD per unit area, Γ is the field effect transistor (FET) channel noise factor, g_m is the FET transconductance, I_2 is the noise bandwidth factor for background noise and I_3 is the noise bandwidth factor.

The SNR at the receiver in the presence of blockages using (22), (23) and (26) can be expressed as:

$$SNR_B = \frac{\left(\mathcal{R} \sum_{i=1}^{N} H_{ij}^B P_{t_i} M_I x_i\right)^2}{\sigma_j^2}, \tag{27}$$

TABLE 1. System model parameters.

Parameter	Value
Room size	5 m × 5 m × 3 m
LED transmitted power	200 mw
Refractive index n	1.5
Optical filter gain T_s	1
Wall reflection ρ	0.8
LED irradiance angle	60°
Receiver plane above the floor (h_R)	0.85 m
Receiver elevation	90°
Receiver active area	1 cm^2
Field of views (FOVs) of receiver	60°.
Blockage radius (r_1 and r_2)	20 cm & 40 cm
Height of the blockage (h_B)	180 cm
Responsivity ($\mathcal{R}$)	0.5 $\frac{\text{A}}{\text{W}}$
Signal bandwidth B_s	10 MHz
Noise bandwidth factor I_2	0.562
Background current I_{bg}	100 μA

By substituting value of H_{ij}^B from (23), it can be rewritten as:

$$SNR_B = \frac{\left[\sum_{i=1}^{N} \sum_{j=1}^{K} \frac{\mathcal{R} M P_{t_i} M_I x_i}{2\pi d_{ij}^2} \exp\left(-2\lambda_B d_{ij} r_B^2\right)\right]^2}{K\sigma_j^2}. \tag{28}$$

For the average SNR calculation, the blockage intensity will be taken as $\lambda_B \in (\lambda_{B_1}, \lambda_{B_2})$ and the blockage radius $r_B \in (r_1, r_2)$ as per the proposed configuration.

VI. RESULTS AND DISCUSSION

In this section, we present the simulation and analytical results for the VLC system with human blockages inside a standard room size of 5 m × 5 m × 3 m. The two transmitter configuration of 4 and 8 LEDs in a rectangular geometry are considered. The locations and the orientations of the VLC transmitters and the receiver are provided in Table 1. Both LoS and NLoS (with one reflection) signals are considered in the analysis.

It may be noted that illumination is considered as a primary functionality of the LEDs and is given priority over communication [35]. To calculate illumination for a VLC system, it is assumed that each LED has a Lambertian radiation pattern, with the Lambert index m, depending on the half-power angle of LED $\Phi_{\frac{1}{2}}$, $m = \frac{-1}{\log_2(\cos \Phi_{\frac{1}{2}})}$. The luminous intensity for LED transmitting power P_t in angle ϕ is given by:

$$I(\phi) = \frac{P_t \cos^m \phi}{4\pi r^2} = I(0)\cos(\phi). \tag{29}$$

where $I(0) = \frac{P_t}{4\pi r^2}$, is the maximum intensity of the flux with angle $\phi = 0°$. A horizontal illuminance E_{hor}, at a point (x,y) is given by:

$$E_{hor} = \frac{I(0)\cos^{m+1}(\phi)}{d^2} \cdot \cos(\theta), \tag{30}$$

where d is the distance between the LED and the receiver surface. For the three-dimensional illumination profile generation, the room floor is divided into grids, and illumination

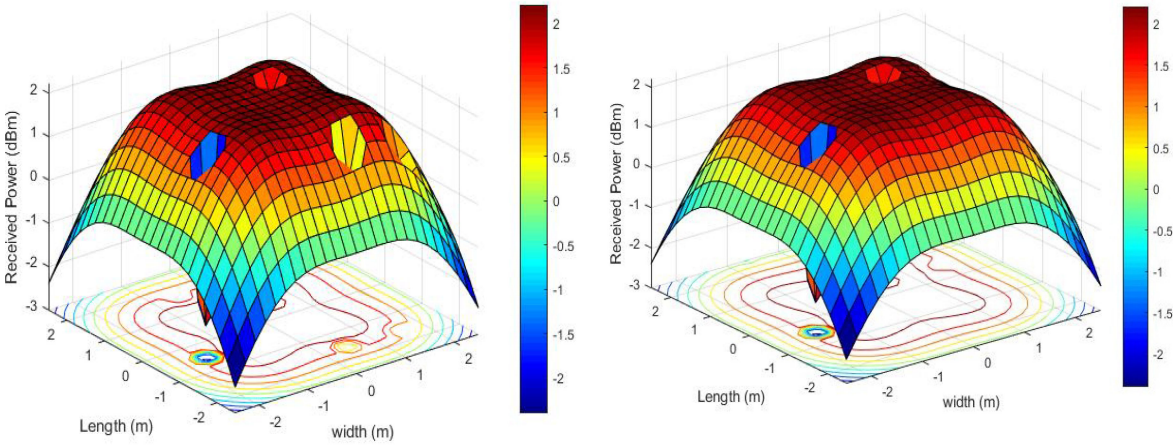

(a) $\lambda_B = 6$. (b) $\lambda_B = 8$.

FIGURE 4. Received optical power distribution profile with human blockage intensity.

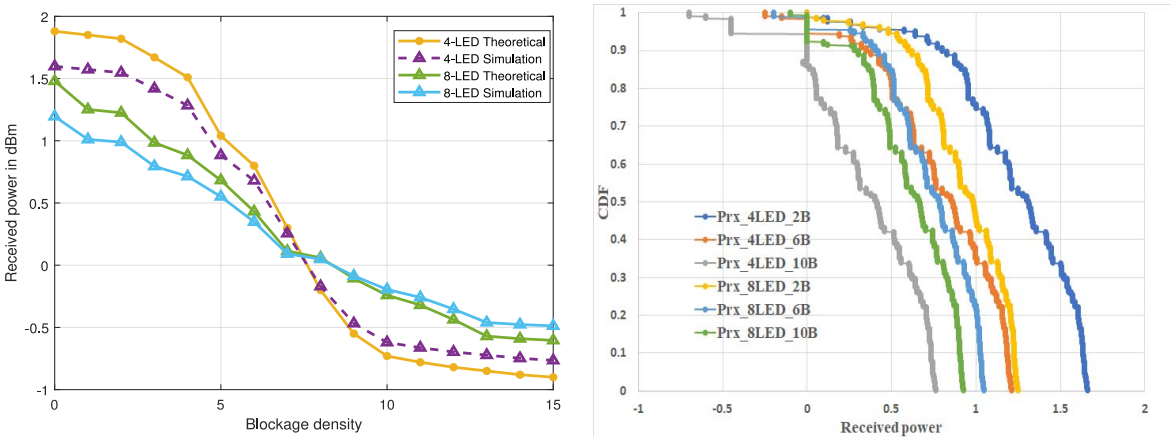

(a) Average received power versus homogeneous blockage density. (b) CDF of average received power of varying homogeneous blockage density.

FIGURE 5. Received power with varying homogeneous blockage intensity.

for each grid using the (30) is calculated. The standard illuminance requirement for indoor room lighting for office work is 300-1500 lux standardized by the international standard organization (ISO), which is fulfilled by the proposed geometry [36]. Hence, from the above discussion, it can be inferred that the proposed work does not compromise the illuminance.

A. RECEIVED SNR PROFILE WITH HUMAN BLOCKAGE

In this subsection, the received SNR profile with human blockages inside the room has been plotted. Figs. 4(a) and 4(b) show the received SNR profile with 4 LEDs having 6 and 8 human blockages of the same radius inside the room. It can be seen that there is a sudden fall in the received SNR whenever there is a blockage between the transmitting LED and the user inside the room. Based upon the distance of blockage from the transmitting LED, its shadow region has been calculated using Fig. 2. As the distance from LEDs to the blockage increases using (8), it can be shown that the shadow region also decreases and vice versa. This results in different size areas of received SNR profile in shadowing due to the blockage and can also be seen in Figs. 4(a) and 4(b).

Further, to see the effect of human blockages of the same and different sizes for 4 and 8 LED configurations, we have calculated the received optical power with increasing blockage intensity discussed in the next subsections.

B. RECEIVED POWER WITH VARYING HOMOGENEOUS BLOCKAGE INTENSITY

Figs. 5(a) and 5(b) show the average received power and CDF of the received power with varying homogeneous blockages intensity inside the room. The human blockages of the same radius $r_1 = 20$ cm has been considered. Fig. 5(a) shows the average received power across the room with increasing blockage intensity with 4-LED and 8-LED in a rectangular configuration. The theoretical and simulation results are in good agreement with each other, validating the mathematical derivations and justifying the approximation made in (28).

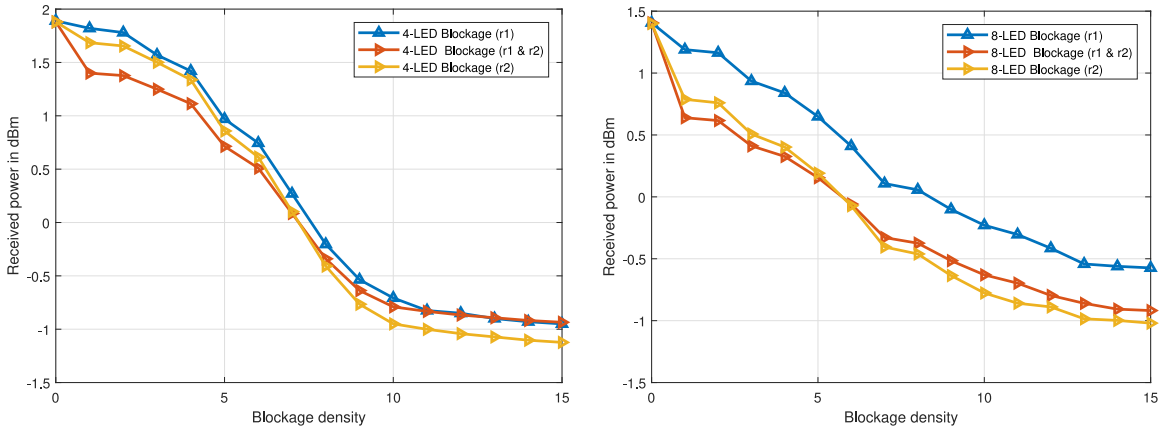

(a) MHCP with 4 LEDs (b) MHCP with 8 LEDs

FIGURE 6. **Average Received power with varying heterogeneous blockage density inside the room with 4 and 8 LEDs.**

It may be noted that in order to satisfy the total power constraint and support the fairness among the different configurations, we have used the constant power of 2 Watts for both 4 and8 LEDs configuration. Thus the per LED transmit power is more in 4 LED configurations, i.e., 0.5 Watt, whereas for the case of 8 LEDs, it is 0.25 Watt. Further, the received power also depends on the relative distance between the LEDs. As mentioned before, the LEDs are placed in rectangular geometry, so in 4 LEDs, the LEDs are separated by more distance with respect to 8 LEDs configuration. In sparse blockages, 4 LEDs provide higher received power because of good line-of-sight (LOS) condition, which means that more LEDs are blocked in 8 LEDs with respect to 4 LEDs. On the contrary, when the number of blockages increases, in 4 LEDs case, the probability of users in LOS with LED decreases, while for 8 LEDs, this probability increases due to spatial diversity (i.e., because of more number of LEDs) so in 8 LEDs case the received power is more as compared to 4 LEDs.

To validate the above argument, we have plotted the received power CDF with 4 and 8 LED configurations in Fig. 5(b). Fig. 5(b) respectively shows that the probability of the received optical power being less than some threshold. For instance, at the probability of 0.5, the received optical power in 4 and 8 LED configurations with two blockages inside the room are 0.5 dBm and 1.23 dBm, respectively. Similarly, as blockage density increases, the 8 LED configuration performs better than the 4 LED, which confirms that the obtained CDF profile in 5(b) is in agreement with the results obtained in Fig. 5(a).

C. RECEIVED POWER WITH HETEROGENEOUS BLOCKAGE INTENSITY USING MHCP

This subsection shows the average received optical power across the room with increasing heterogeneous blockage density for 4-LED and 8-LED configuration. Two size of blockages with radius r_1 and r_2 have been considered, where $r_1 < r_2$. Figs. 6(a) and 6(b) show the average received power with heterogeneous blockage intensity inside the room with 4 and 8 LEDs, respectively. The blockages are realized using (17) MHCP process with radius r_1, r_2 and mix radii (r_1 and r_2), equal number blockages have been realized for each case with equal probability. For example, in heterogeneous blockage realization, both r_1 and r_2 radius blockages have been realized with equal probability. The average received power is decreasing with respect to the increasing blockage density. It is evident from the figure that the homogeneous blockages with radius r_1 are performing best among blockage with radius r_2 and mix radii. It is interesting to observe that for lower blockage density, blockage with mixed radii is performing better than the blockage with radius r_2. However, this trend is reversed for higher blockage density (more than 7), as shown in Figs. 6(a) and 6(b). It is due to the fact that during the realization of blockages using the MHCP process, the less number of blockages are realized with radius r_2 in comparison to mix radii because of wider radius and thinning process in MHCP.

Further, it can also be observed from Fig. 6 that 4-LED configuration is giving better average received power compared to the 8-LED configuration for constant transmit power of 2 Watts for each configuration. However, for the higher blockage density of r_2 and mix radii, the 8-LED configuration gives better performance than the 4-LED configuration.

D. RECEIVED POWER WITH HETEROGENEOUS BLOCKAGE INTENSITY USING RWP

In this subsection, we have shown the average received optical power results across the room with heterogeneous blockage density using the RWP model. Figs. 7(a) and 7(b) show the average received optical power with varying blockage intensity inside the room with 4 and 8 LEDs, respectively. The blockages are realized using RWP mobility model with radius r_1, r_2 and mix radii. It can be observed that the blockage with radius r_1 is performing better than the r_2 and mix radii for both 4-LED and 8-LED configuration.

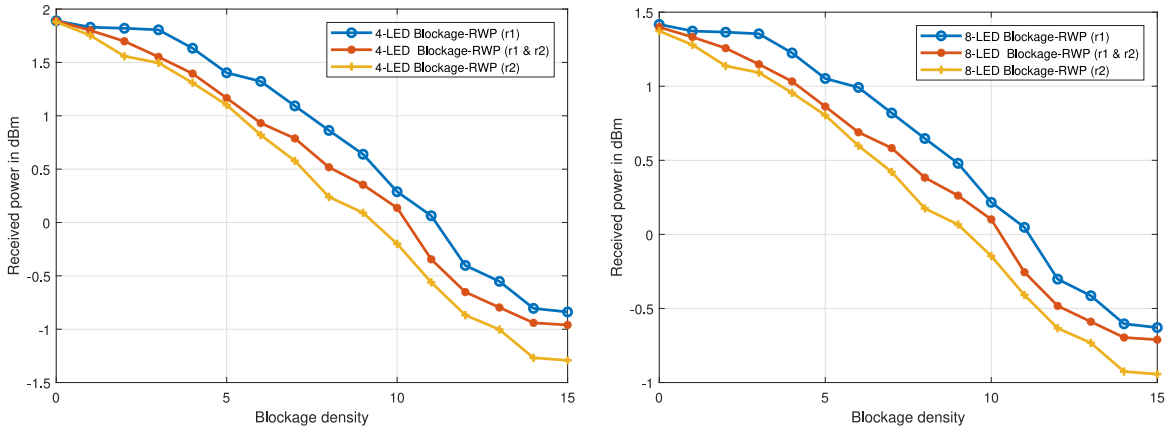

(a) MHCP with 4 LEDs (b) MHCP with 8 LEDs

FIGURE 7. **Average Received power with varying heterogeneous blockage density inside the room with 4 and 8 LEDs using RWP.**

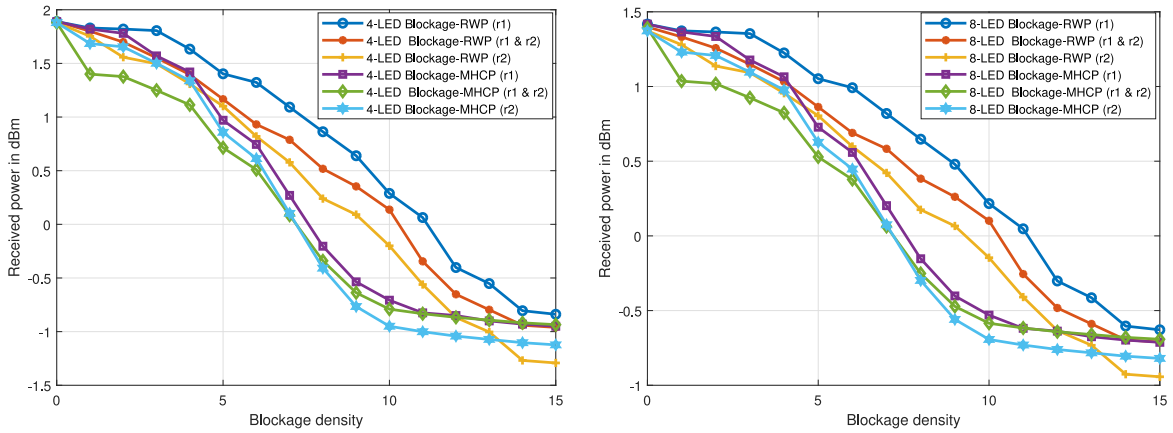

(a) MHCP with 4 LEDs (b) MHCP with 8 LEDs

FIGURE 8. **Comparison of average Received power with heterogeneous blockage density inside the room with 4 and 8 LEDs using MHCP and RWP.**

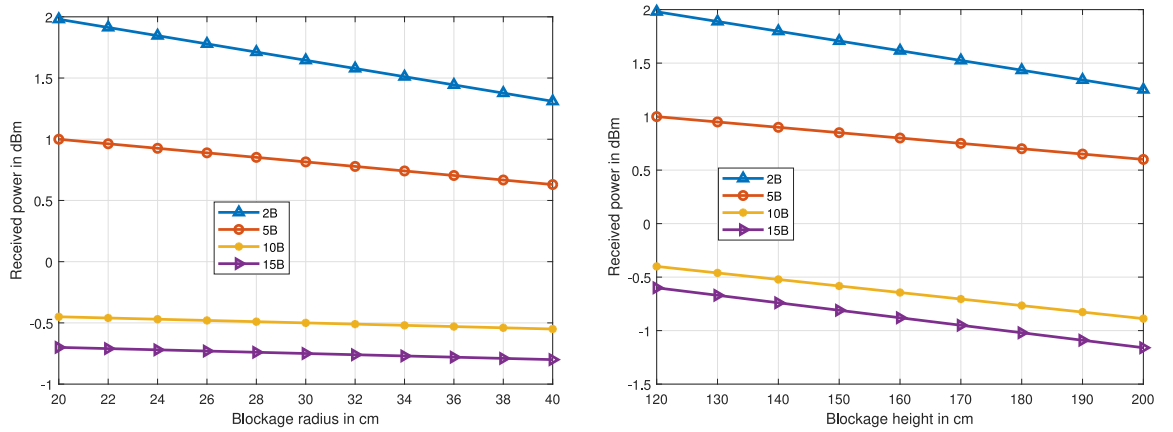

(a) Received power versus varying blockage radius (b) Received power versus varying blockage heights

FIGURE 9. **Average received power with varying blockage height and radius.**

There is no crossover between r_2 and mix radii blockage realization using MHCP, and there is a clear gap between the received optical power in larger and smaller blockages.

Fig. 8 shows the comparison of average received optical power with heterogeneous blockage density inside the room with 4 and 8 LEDs using MHCP and RWP. It can

be observed from Fig. 8(a) that average received power is decreasing with an increase in blockage density for both MHCP and RWP. The average received power with RWP performs slightly better than the MHCP because in the RWP model using (19), the user probability of being in the center is more than in edges or anywhere in the room, which results in a less number of LEDs getting blocked in a rectangular configuration. Further, the average received power with the RWP model is continuously decreasing for higher blockage density, while for MHCP, the average power gets saturated for higher blockage density due to the stationary behavior of the MHCP.

E. RECEIVED POWER WITH VARYING BLOCKAGE RADIUS AND HEIGHT

In this section, we have plotted the received power for different height and width of the human blockages, as shown in Fig. 9. It may be noted that for modelling static human blockages, we have used the Matern hardcore point process (MHCP). For the width of the human blockage, the radius has been varied from 20 cm to 40 cm to reflect a typical human's waist size, as shown in Fig. 9(a). It can be observed that the received power decreases as the human blockages' width increases for different blockage densities. However, for lower number human blockage, the reduction is more as compared to higher human number blockage.

Similarly, the height of blockage has been varied from 120 cm to 200 cm to reflect human height, as shown in Fig. 9(b). It can be observed that the received power decreases as the height of the human blockages increases due to the larger shadow of the blockages.

VII. CONCLUSION

In this letter, the performance of an indoor VLC system with human blockages have been analyzed. For the realization of static and dynamic blockages inside the room, the MHCP and RWP model are used, respectively. We have also calculated the blockage intensity profile for homogeneous and heterogeneous blockage density as well as the analytical expression of the received SNR for varying size human blockages inside the room using MHCP. The analytical results are in close agreement with the simulation results, which validates the analytical framework proposed in this article. The received SNR profile shows the effect of shadowing in terms of a decrease in received SNR at the blockages' locations. The received optical power with an increasing number of human blockage intensity of varying sizes with 4-LED and 8-LED configuration has also been plotted. Further, the effect of varying human height and width also have been analyzed. It can be observed that the received power decreases as the human blockages' width increases for different blockage densities. However, for lower number human blockage, the reduction is more as compared to higher human number blockage. It is concluded that for the higher number of blockages, the 8-LED configuration has been shown to perform better as compared to 4-LED for the same amount of total power from transmitting LEDs.

REFERENCES

[1] L. Feng, R. Q. Hu, J. Wang, P. Xu, and Y. Qian, "Applying VLC in 5G networks: Architectures and key technologies," *IEEE Netw.*, vol. 30, no. 6, pp. 77–83, Nov./Dec. 2016.

[2] L. Shi, W. Li, X. Zhang, Y. Zhang, G. Chen, and A. Vladimirescu, "Experimental 5G new radio integration with VLC," in *Proc. 25th IEEE Int. Conf. Electron. Circuits Syst. (ICECS)*, Dec. 2018, pp. 61–64.

[3] J. E. Mitchell, "Integrated wireless backhaul over optical access networks," *J. Lightw. Technol.*, vol. 32, no. 20, pp. 3373–3382, Oct. 15, 2014.

[4] A. Khreishah, S. Shao, A. Gharaibeh, M. Ayyash, H. Elgala, and N. Ansari, "A hybrid RF-VLC system for energy efficient wireless access," *IEEE Trans. Green Commun. Netw.*, vol. 2, no. 4, pp. 932–944, Dec. 2018.

[5] T. Komine and M. Nakagawa, "Fundamental analysis for visible-light communication system using LED lights," *IEEE Trans. Consum. Electron.*, vol. 50, no. 1, pp. 100–107, Feb. 2004.

[6] J. Grubor, S. Randel, K.-D. Langer, and J. W. Walewski, "Broadband information broadcasting using LED-based interior lighting," *J. Lightw. Technol.*, vol. 26, no. 24, pp. 3883–3892, Dec. 15, 2008.

[7] A. Jovicic, J. Li, and T. Richardson, "Visible light communication: Opportunities, challenges and the path to market," *IEEE Commun. Mag.*, vol. 51, no. 12, pp. 26–32, Dec. 2013.

[8] D. Karunatilaka, F. Zafar, V. Kalavally, and R. Parthiban, "LED based indoor visible light communications: State of the art," *IEEE Commun. Surveys Tuts.*, vol. 17, no. 3, pp. 1649–1678, 3rd Quart., 2015.

[9] H. Elgala, R. Mesleh, and H. Haas, "Indoor optical wireless communication: Potential and state-of-the-art," *IEEE Commun. Mag.*, vol. 49, no. 9, pp. 56–62, Sep. 2011.

[10] H. Tabassum and E. Hossain, "Coverage and rate analysis for co-existing RF/VLC downlink cellular networks," *IEEE Trans. Wireless Commun.*, vol. 17, no. 4, pp. 2588–2601, Apr. 2018.

[11] B. G. Guzman, A. L. Serrano, and V. P. Gil Jimenez, "Cooperative optical wireless transmission for improving performance in indoor scenarios for visible light communications," *IEEE Trans. Consum. Electron.*, vol. 61, no. 4, pp. 393–401, Nov. 2015.

[12] Y. U. Lee and M. Kavehrad, "Two hybrid positioning system design techniques with lighting LEDs and ad-hoc wireless network," *IEEE Trans. Consum. Electron.*, vol. 58, no. 4, pp. 1176–1184, Nov. 2012.

[13] M. Gapeyenko *et al.*, "Analysis of human-body blockage in urban millimeter-wave cellular communications," in *Proc. IEEE Int. Conf. Commun. (ICC)*, 2016, pp. 1–7.

[14] M. A. Dastgheib, H. Beyranvand, and J. A. Salehi, "Optimal visible light communication access point placement under stationary distribution of users' mobility," in *Proc. 9th Int. Symp. Telecommun. (IST)*, 2018, pp. 96–101.

[15] C. Bettstetter, H. Hartenstein, and X. Pérez-Costa, "Stochastic properties of the random waypoint mobility model," *Wireless Netw.*, vol. 10, no. 5, pp. 555–567, 2004.

[16] M. A. Dastgheib, H. Beyranvand, J. A. Salehi, and M. Maier, "Mobility-aware resource allocation in VLC networks using T-step look-ahead policy," *J. Lightw. Technol.*, vol. 36, no. 23, pp. 5358–5370, Dec. 1, 2018.

[17] L. Feng, R. Q. Hu, J. Wang, and Y. Qian, "Deployment issues and performance study in a relay-assisted indoor visible light communication system," *IEEE Syst. J.*, vol. 13, no. 1, pp. 562–570, Mar. 2019.

[18] P. Fulop, S. Szabo, and T. Szalka, "Accuracy of random walk and Markovian mobility models in location prediction methods," in *Proc. 15th Int. Conf. Softw. Telecommun. Comput. Netw.*, 2007, pp. 1–5.

[19] X. Hong, M. Gerla, G. Pei, and C.-C. Chiang, "A group mobility model for ad hoc wireless networks," in *Proc. 2nd ACM Int. Workshop Model. Anal. Simulat. Wireless Mobile Syst.*, 1999, pp. 53–60.

[20] I. Rhee, M. Shin, S. Hong, K. Lee, S. J. Kim, and S. Chong, "On the levy-walk nature of human mobility," *IEEE/ACM Trans. Netw.*, vol. 19, no. 3, pp. 630–643, Jun. 2011.

[21] F. Ashtiani, J. A. Salehi, and M. R. Aref, "Mobility modeling and analytical solution for spatial traffic distribution in wireless multimedia networks," *IEEE J. Sel. Areas Commun.*, vol. 21, no. 10, pp. 1699–1709, Dec. 2003.

[22] G. H. Mohimani, F. Ashtiani, A. Javanmard, and M. Hamdi, "Mobility modeling, spatial traffic distribution, and probability of connectivity for sparse and dense vehicular ad hoc networks," *IEEE Trans. Veh. Technol.*, vol. 58, no. 4, pp. 1998–2007, May 2009.

[23] T. Camp, J. Boleng, and V. Davies, "A survey of mobility models for ad hoc network research," *Wireless Commun. Mobile Comput.*, vol. 2, no. 5, pp. 483–502, 2002.

[24] B. Matérn, *Spatial Variation*, vol. 36. Cham, Switzerland: Springer, 2013.

[25] I. Stefan and H. Haas, "Analysis of optimal placement of led arrays for visible light communication," in *Proc. IEEE 77th Veh. Technol. Conf. (VTC Spring)*, 2013, pp. 1–5.

[26] S. Rajagopal, R. D. Roberts, and S.-K. Lim, "IEEE 802.15. 7 visible light communication: Modulation schemes and dimming support," *IEEE Commun. Mag.*, vol. 50, no. 3, pp. 72–82, Mar. 2012.

[27] F. R. Gfeller and U. Bapst, "Wireless in-house data communication via diffuse infrared radiation," *Proc. IEEE*, vol. 67, no. 11, pp. 1474–1486, Nov. 1979.

[28] W.-T. Chien, C.-C. Sun, and I. Moreno, "Precise optical model of multi-chip white LEDs," *Opt. Exp.*, vol. 15, no. 12, pp. 7572–7577, 2007.

[29] Y. Qiu, H.-H. Chen, and W.-X. Meng, "Channel modeling for visible light communications—A survey," *Wireless Commun. Mobile Comput.*, vol. 16, no. 14, pp. 2016–2034, 2016.

[30] M. Jacob *et al.*, "Fundamental analyses of 60 GHz human blockage," in *Proc. 7th Eur. Conf. Antennas Propag. (EuCAP)*, 2013, pp. 117–121.

[31] S. N. Chiu, D. Stoyan, W. S. Kendall, and J. Mecke, *Stochastic Geometry and Its Applications*. Hoboken, NJ, USA: Wiley, 2013.

[32] M. Månsson and M. Rudemo, "Random patterns of nonoverlapping convex grains," *Adv. Appl. Probabil.*, vol. 34, no. 4, pp. 718–738, 2002.

[33] I. Neokosmidis, T. Kamalakis, J. W. Walewski, B. Inan, and T. Sphicopoulos, "Impact of nonlinear LED transfer function on discrete multitone modulation: Analytical approach," *J. Lightw. Technol.*, vol. 27, no. 22, pp. 4970–4978, Nov. 15, 2009.

[34] L. Hua, Y. Zhuang, L. Qi, J. Yang, and L. Shi, "Noise analysis and modeling in visible light communication using allan variance," *IEEE Access*, vol. 6, pp. 74320–74327, 2018.

[35] T.-C. Bui, S. Kiravittaya, K. Sripimanwat, and N.-H. Nguyen, "A comprehensive lighting configuration for efficient indoor visible light communication networks," *Int. J. Opt.*, vol. 2016, Dec. 2016, Art. no. 8969514.

[36] I. Din and H. Kim, "Energy-efficient brightness control and data transmission for visible light communication," *IEEE Photon. Technol. Lett.*, vol. 26, no. 8, pp. 781–784, Apr. 15, 2014.